Journal of X-Ray Science and Technology 19 (2011) 155–172
DOI 10.3233/XST-2011-0284
IOS Press

Reconstruction from truncated projections using mixed extrapolations of exponential and quadratic functions

Shuangren Zhao[a,*], Kang Yang[b] and Xintie Yang[c]
[a]*Doubletask North York, Ontario, Canada*
[b]*University of Toronto, Toronto, Canada*
[c]*Northwestern Poly Technical University Xian, Xian, China*

Received 14 July 2010
Revised 23 January 2011
Accepted 31 January 2011

Abstract. In computer tomography (CT), truncated projections are produced due to scanning large objects with a detector that is limited in width. Applying filtered back-projection(FBP) method directly to truncated projections, the reconstructed image will contain truncation artifacts – bright rings on the boundary of region of interest (ROI). Extrapolation algorithms can be used to reduce the truncation artifacts; however extrapolations are usually double the length of the projection data; resulting in an increased calculation time. This paper introduces mixed extrapolation, which is a combination of exponential and quadratic extrapolation. It is proven that doubling the length of the projection data for the mixed extrapolation can be avoided. The projections were extrapolated according to the boundary values and their derivatives. The algorithm achieves equivalence to the extrapolation approach with negligible increased calculation time. Supplementary functions are introduced in order to simplify the calculations. These functions can be calculated prior to extrapolation process, hence the calculation time is significantly reduced. The calculation times are compared between fast extrapolation introduced in this paper and normal extrapolation with doubling the length of projection data.

Keywords: Extrapolation, truncation artifacts, truncated projections, local tomography, limit field of view, reconstruction, incomplete projections, quadratic, exponential

1. Introduction

Many fan-beam and cone-beam reconstruction methods [1,4,2,3,16,17] used for complete (truncation free) projection data, among therm those published recently are [22–24,27]. There are two kind of truncation problem for the image reconstruction: interior problem and exterior problem. If the ROI corresponding to the FOV has holes, it is exterior problem. For example, the metal substances can produce severe beam harden artifacts in the reconstructed image, they are often taken away from projection data and hence leave a hole on the ROI. The article [25] discussed exterior problem. Interior problem is also called limited-field-of-view(LFOV) problem which will be discussed in details.

*Corresponding author: Shuangren Zhao, Doubletask North York, Ontario, Canada. E-mail: shrzhao@rogers.com.

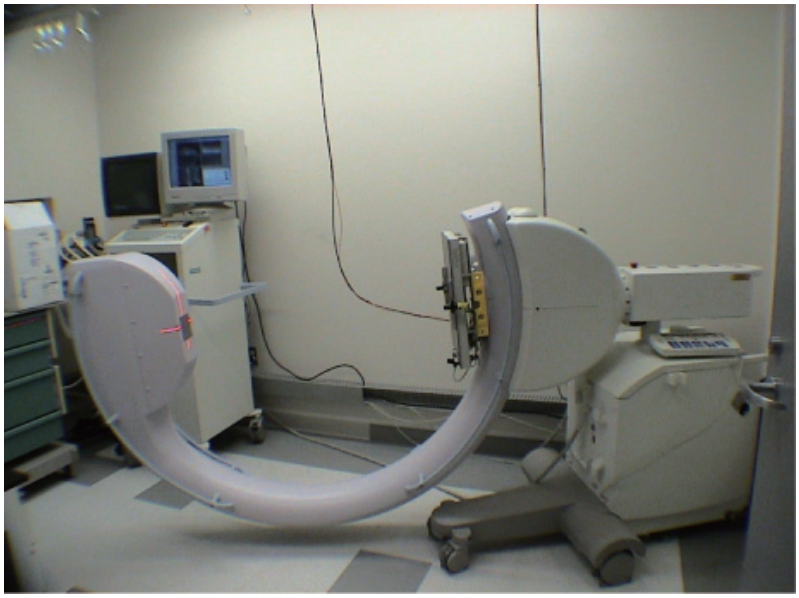

Fig. 1. Siemens Isocentric C-arm with Integrated cone-beam CT.

Currently, Siemens isocentric C-arm with integrated cone-beam CT (Fig. 1) with flat panel detector [5] is used. The field of view (FOV) of 21 cm is limited to the width of the detector (40 cm); therefore, the projections are truncated. This is referred to as limited field of view (LFOV) problem. Reconstruction using truncated projections often result in truncation artifacts; bright rings on the boundary of the region of interest (ROI). Here it is assumed that the ROI corresponds to the FOV of the detector, resulting in the absence of a margin between the ROI and FOV. 3i.e. the diameter of the ROI is equal to the width of the FOV.

The truncation problem with the offset detector was solved by using iterative reconstruction-reprojection method and pre- or post-convolution methods [9]. Moreover, an additional half scan is required for these methods. The difficulty of this kind of truncation problem is data redundancy, because the two half scans overlap. If only a half scan is available, the truncated projections are incomplete data. Then the problem is LFOV.

Local tomography [6] and wavelet methods [7,8] are normally used to reduce truncation artifacts. Local tomography, a type of frequency filter method function by filtering out low frequency values and reserve the high frequency values for the reconstructed image. High frequency values are less influenced through the truncated projections; whereas, low frequency values are more influenced through the truncated projections. Local tomography can reduce truncation artifacts; however the trade-off is that local tomography looses the low frequency values of the reconstructed image. Wavelet methods are often used in conjunction with extrapolation [7,8]. Rashid-Farrokhi has found that, it is not the wavelets that are important to reduce the truncation artifacts, rather an extrapolation of the local data [7].

Utilizing a priori for the LFOV problem was studied by Ruchala [11]. If the part of ROI lies outside of the object, the Hilbert transform method [10,20,26,28] can give a solution for the LFOV problem. An efficient correction for truncation artifacts was shown by B. Ohnesorge [13]. An iterative algorithm for LFOV can be seen by [14,15].

Although there are many different methods that are even more suitable to LFOV problem, extrapolation method still widely uses because of simplicity. Usually the length of projection data will be doubled

after the extrapolation, which will increase the calculation time. The problem of increasing calculation time was not a critical for cone-beam CT image reconstruction using FBP method because the filtering process was much faster compare to the back-projection process. However, it is more serious now because the fast back-projection algorithm [18,21] is available. A fast calculation algorithm for linear and constant extrapolation was mentioned by [14] without given the details. The calculation using this algorithm requires almost the same calculation time as using the algorithm without extrapolations.

Many different sophisticated functions can be utilized as extrapolation functions with better ability to reduce the truncation artifacts compared to constant or linear extrapolation. A study of LFOV using cosine extrapolations was shown by Magnussonc [12]. The author of this article has attempted to avoid doubling the length of projection data for cosine extrapolation, however it did not succeed. Mixed extrapolation functions are created in this paper so that it is not only with better ability to reduce the truncation artifacts but also to avoid doubling the length of projection data. Here the mixed extrapolation function is a combination of a quadratic function and an exponential function.

It is worth to notice that, since normally the calculation time for the FBP reconstruction is mostly spent at back-projection step, avoiding the doubling the projection data cannot offer much speedup for a combined process with filtering and back-projection. However if fast back-projection algorithms [18,21] are utilized, the filtering process will have the same order of calculation time with the back-projection process. Only in this situation the speedup from avoiding the doubling the projection data is distinct. It also worth to know that with mixed extrapolation alone, the effect of reducing truncation artifacts are limited especially when there is massive object outside the ROI. Combining mixed extrapolation with one iteration can significantly improve the ability to reduce the truncation artifacts [15]. In the next section the development of the algorithm for mixed extrapolation is done.

2. Development of the algorithm

2.1. Extrapolation of the projections

In the cone-beam reconstruction, projections are weighted according to their cone-beam angle [1]. After the weighting process has been applied, the projections are ready for the filter process. Suppose that

$$p(i) \qquad i = 0, 1, \cdots N-1 \tag{1}$$

expresses the projection data before the filtering process. Here i is the projection column element index. To simplify the expression, we omit two other variables for cone-beam projections: rotating angle and row element index. Here row index is along the direction of rotation axis. $i = 0$ is the leftmost element of the projection and $i = N-1$ is the rightmost element of the projection. The extrapolation did not require utilizing all the projection data available. We can make extrapolation at any place j, k satisfying

$$-1 \leqslant k < j \leqslant N \tag{2}$$

Define the boundary value as:

$$R_+ \equiv p(j-1) \tag{3}$$

$$S_+ \equiv \frac{\partial}{\partial i} p(i)|_{i=j-1} \tag{4}$$

where j is the beginning of the extrapolation on the right side, and $j-1$ is the place where we take the initial value for the extrapolation. Here the symbol $\frac{\partial}{\partial i}$ is not the exact derivative, since the data is discrete. $\frac{\partial}{\partial i}$ will be defined and calculated in later in Section 2.3. In the same way define the boundary value on the left side as:

$$R_{-} \equiv p(k+1) \tag{5}$$

$$S_{-} \equiv \frac{\partial}{\partial(-i)} p(i)|_{i=k+1} \tag{6}$$

where k is the beginning of the extrapolation on the left side and $k+1$ is the place taking the initial value for the extrapolation on the left side. If all projection data is utilized, there are:

$$j = N \tag{7}$$

$$k = -1 \tag{8}$$

If Eqs (7) and (8) are not satisfied (i.e. $-1 < k < j < N$) then the projections are artificially truncated even they themselves are not truncated after the measurement. Artificially truncated projections were used to study the algorithm for the problem of LFOV.

Define a door function:

$$\Pi_L(i) = \begin{cases} 1 \text{ if } i \geqslant 0 \text{ and } i \leqslant L \\ 0 \text{ if } i < 0 \text{ and } i > L \end{cases} \tag{9}$$

where L is the length of extrapolation (can be defined by the user according to the scale of the object to be reconstructed) and L is usually taken as half of the number of the elements of the projections:

$$L = \frac{N}{2} \tag{10}$$

Considering two sides of extrapolations the length of projection data is doubled.

2.2. The contribution of the extrapolation

The filter function is written as $h(i)$, which is symmetrical [19]. The quadratic extrapolated projections on the right side can be written as:

$$p_{+}(i) = \Pi_L(i-j)[a_{+}(i-(j-1))^2 + b_{+}(i-(j-1)) + c_{+}] \tag{11}$$

The nonzero values of this function begins at j and ends at $j+L$. In the above formula c_{+},b_{+} can be obtained from the initial values Eqs (3, 4, 5 and 6):

$$c_{+} = R_{+} \tag{12}$$

$$b_{+} = S_{+} \tag{13}$$

The details about R_{+}, S_{+} are given in Section 2.3. Choosing the right side of the Eq. (11) as zero when $i = j+L$, the value of a_{+} can be obtained (Appendix 1):

$$a_{+} = -\frac{b_{+}(L+1) + c_{+}}{(L+1)^2} \tag{14}$$

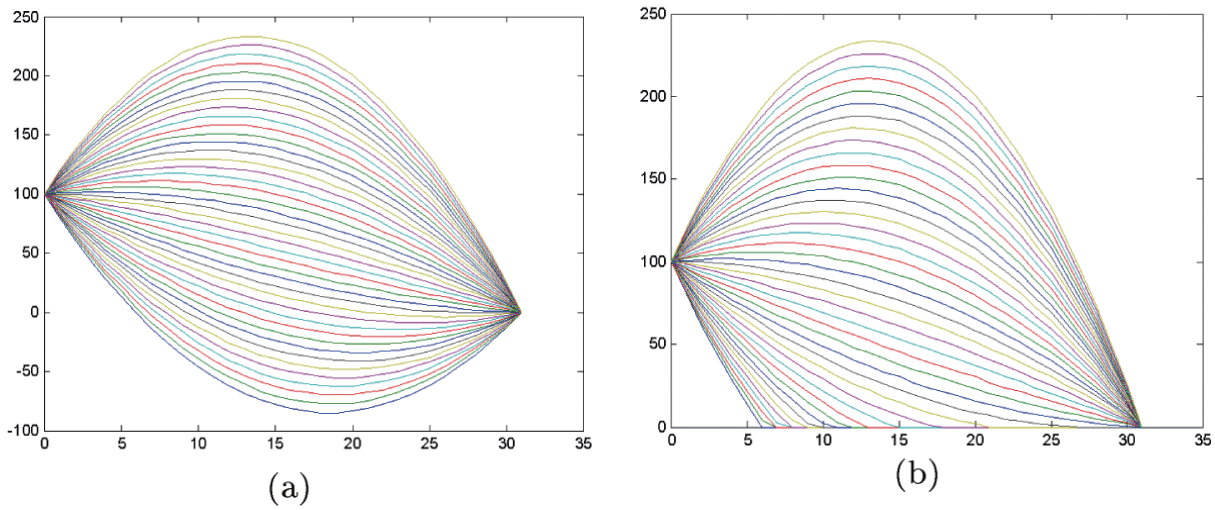

Fig. 2. (a) With different initial value b_+, the quadratic extrapolation functions are with negative values. (b) The quadratic extrapolations are set to zero for all negative values.

The extrapolation functions Eq. (11) can be seen in Fig. 2a and contains negative values. Negative values are not realistic for projections; hence, all of negative values are set to zero. This can be achieved through solving the following equation at $l = i - (j - 1)$:

$$a_+ l^2 + b_+ l + c_+ = 0. \tag{15}$$

and set zero for all $i - j > l_+$. Here l_+ is the solution of the above quadratic equation that is:

$$l_+ = \frac{-b_+ - \sqrt{b_+^2 - 4a_+ c_+}}{2a_+} \tag{16}$$

If the above value is smaller than L, L should be replaced by l_+. Define

$$L_+ = \begin{cases} l_+ \text{ if } \mathrm{l}_+ < \mathrm{L} \\ L \text{ else} \end{cases} \tag{17}$$

To distinguish L_+ with L, L_+ is referred as the practical extrapolation length on the right side. In the Eq. (11) L should be replaced by L_+:

$$p_+(i) = \Pi_{L_+}(i - j)[a_+(i - (j - 1))^2 + b_+(i - (j - 1)) + c_+] \tag{18}$$

The quadratic extrapolation functions Eq. (18) are set to zero for all negative values; see Fig. 2b.

Linear extrapolation and constant extrapolation can be made as special cases of quadratic extrapolation. It can be done by letting $a_+ = 0$ and $b_+ = 0$ on the Eq. (11) or Eq. (18) for constant extrapolation.

In practice, the reconstruction for LFOV is improved using quadratic extrapolation than the reconstruction using constant extrapolation or liner extrapolation. However the reconstruction using quadratic extrapolation is still not perfect. The extrapolated projections using quadratic extrapolation usually have

much higher values than real projections. In order to reduce the values of extrapolated projections, a modification of quadratic extrapolation with exponential functions is shown in the following:

$$p_+^{(m)}(i) = p_+(i)\ \exp\left(-\left(\frac{i-j}{\alpha L}\right)^m\right) \tag{19}$$

where α is a parameter (values are $0.0 \sim 1$). $m = 0, 1, 2, \ldots$. $p_+^{(0)}(i) = p_+(i)$ is quadratic extrapolation. In this paper the situation where $m = 0$, 1, 2 is considered only. There is fast calculation algorithm for $m = 0$, 1, which will be given in the following. For $m = 2$, it is difficult to make a fast calculation; doubling the size of projection elements is required. $p_-(i)$ and $p_-^{(m)}(i)$ are the extrapolation of projection functions on the left side, which can be obtained similar to the right side because of the symmetry of the system. The extrapolated projections can be written as

$$p_e(i) = p(i) + p_+^{(m)}(i) + p_-^{(m)}(i) \tag{20}$$

where $p(i)$ is truncated projection. The contribution of the filter process from extrapolated projections g_e is

$$g_e(i) = (h \star p)(i) + g_-(i) + g_+(i) \tag{21}$$

where "$\star$" represents convolution. $i \in [k+1, j-1]$. Truncated projections is given as $p(i)$. $g_-(i)$ and $g_+(i)$ are the contribution of the extrapolation, which are defined as

$$g_\pm(i) = (h \star p_\pm^{(m)})(i) \tag{22}$$

where $g_\pm$ represents either g_- or g_+. For $m = 0$,1, $g_\pm(i)$ can be directly calculated, which avoids doubling the size of projections. For this purpose, supplementary functions are defined as:

$$G^{(p)}(s) = \sum_{n=s}^{M} n^p \exp\left(-\left(\frac{n}{\alpha L}\right)^m\right) \tag{23}$$

where $m = 0, 1$. $p = 0, 1, 2$. M should be taken large enough, for example

$$M \geqslant N + L + (N - j) + 1 \tag{24}$$

A second supplementary function is defined as:

$$G_L^{(p)}(t) = \sum_{n=t}^{t+L} n^p \exp\left(-\left(\frac{n}{\alpha L}\right)^m\right) \tag{25}$$

The relationship between Eqs (23) and (25) is:

$$G_L^{(p)}(t) = G^{(p)}(t) - G^{(p)}(t + L + 1) \tag{26}$$

Using these supplementary functions, Eq. (22) can be calculated directly. The results (see Appendix 2.) are shown here:

$$g_\pm(i) = \left[A_\pm G_{L_\pm}^{(2)}(t_\pm) + B_\pm G_{L_\pm}^{(1)}(t_\pm) + C_\pm G_{L_\pm}^{(0)}(t_\pm)\right] \exp\left(\left(\frac{t_\pm}{\alpha L}\right)^m\right) \tag{27}$$

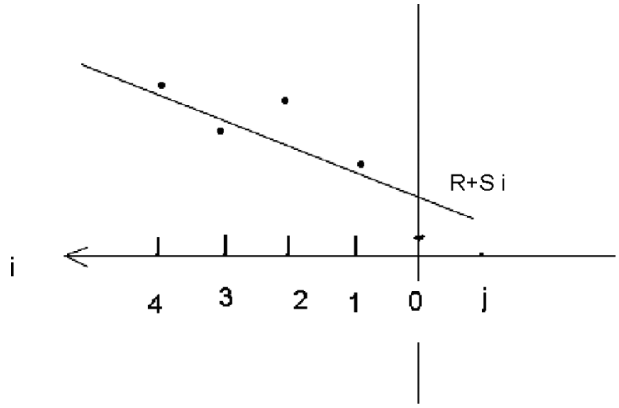

Fig. 3. Example of line fitting using 5 points for the extrapolation in the right side.

where

$$A_{\pm} = a_{\pm} \tag{28}$$

$$B_{\pm} = 2a_{\pm}(1 - t_{\pm}) + b_{\pm} \tag{29}$$

$$C_{\pm} = a_{\pm}(1 - t_{\pm})^2 + b_{\pm}(1 - t_{\pm}) + c_{\pm} \tag{30}$$

$$t_{+} = j - i \tag{31}$$

$$t_{-} = i - k \tag{32}$$

Similar to Eqs (14), (16) and (17) taking the symmetry into consideration, we have the following formula,

$$a_{-} = -\frac{b_{-}(L+1) + c_{-}}{(L+1)^2} \tag{33}$$

$$l_{-} = \frac{-b_{-} - \sqrt{b_{-}^2 - 4a_{-}c_{-}}}{2a_{-}} \tag{34}$$

$$L_{-} = \begin{cases} l_{-} \text{ if } \mathrm{l}_{-} < \mathrm{L} \\ L \text{ else} \end{cases} \tag{35}$$

2.3. Calculation of the initial values $R_{\pm}S_{\pm}$

There are two choices for extrapolations, a) setting the slope of projections at extrapolation point as 0; b) considering the slope of projections. In situation a) there are:

$$R_{+} = p(j - i) \tag{36}$$

$$S_{+} = 0 \tag{37}$$

In the situation b), the slope of projections are considered. For simplicity, this can be done by choosing the formula: $R_+ = p(j-1)$, $S_+ = p(j-1) - p(j-2)$, using the two points fit. However because the projections oscillate strongly, S_+ obtained this way are not very satisfactory. To overcome this difficulty, the minimal norm fit method with 5 points (here 5 is taken arbitrarily means few points, 4 or 6 is also OK) close to the boundary of ROI is utilized to find the boundary values (Appendix 3),

$$R_\pm = 0.6F_1 - 0.2F_2 \tag{38}$$

$$S_\pm = 0.2F_1 - 0.1F_2 \tag{39}$$

where

$$F_1 = \sum_{i=o}^{4} f(i) \tag{40}$$

$$F_2 = \sum_{i=1}^{4} i\, f(i) \tag{41}$$

where

$$f(i) = \begin{cases} p(-(i-(j-1))) & \text{for the right side} \\ p(i-(k+1)) & \text{for the left side} \end{cases} \quad i = 0,1,2,3,4 \tag{42}$$

In the Eqs (36,37,38,39) the subscript "+" for $R_\pm$ and $S_\pm$ correspond to the right side; the subscript "$-$" for $R_\pm$ and $S_\pm$ correspond to the left side.

Comparing this two choices, the advantage of choice a) is that it has less influence from the noise data and the advantage b) is that it utilized the slope information of the projection data, hence batter at reducing the truncation artifacts.

2.4. The relation of the values between $b_\pm$, $c_\pm$ and $R_\pm$, $S_\pm$

After adding an exponential fact to the quadratic extrapolation formula $b_\pm$ is not the initial differential value of the Eq. (19). Eq. (13) is not incorrect and corrections should be made. For $m = 1$

$$b_+ = \frac{\partial}{\partial i} p(i)|_{i=j-1} + \frac{R_+}{\alpha L} = S_+ + \frac{R_+}{\alpha L} \tag{43}$$

$$b_- = \frac{\partial}{\partial(-i)} p(i)|_{i=k+1} + \frac{R_-}{\alpha L} = S_- + \frac{R_-}{\alpha L} \tag{44}$$

for $m \neq 1$, the last term of above formula disappear. So that Eq. (13) is replaced as

$$b_\pm = \begin{cases} S_\pm + \frac{R_\pm}{\alpha L} & m = 1 \\ S_\pm & m = 0, 2 \end{cases} \tag{45}$$

Considering the symmetry of the system, rewrite the Eq. (12) as

$$c_\pm = R_\pm \tag{46}$$

2.5. Summary algorithm

For cone-beam FBP reconstruction, the projections are first weighted according to the cone angle [1]; the second is the filtering process; the third is the back-projection process. In the implementation of the mixed extrapolations, the extrapolation process is done on the weighted projections instead on the projections. The filtering process is calculated through Eq. (21). The contribution to the filtered projections from the extrapolation $g_{\pm}(i)$ in Eq. (21) are calculated from Eq. (27). The functions $G_{L_{\pm}}(t)$ in Eq. (27) are calculated through Eq. (26). The functions $G^{(p)}(t)$ in the Eq. (26) are defined in Eq. (23), which can be pre-calculated. This pre-calculation is the key point to save the calculations. The variables M in Eq. (23) is given by Eq. (24). $t_{\pm}$ in Eq. (27) is defined in Eqs (31) and (32). j and k in Eqs (31) and (32) are defined in Eq. (2). $L_{\pm}$ in Eq. (27) is calculated through Eqs (17) and (35). The initial length L of extrapolation in the Eqs (17) and (35) can be given by the user according to the scale of the object. Usually L is chosen as half of the number of the elements of a projection Eq. (10) so that the extrapolated projection just double the length of projections. The variables l_{+} in Eq. (17) and l_{-} in Eq. (35) can be calculated from Eqs (16) and (34). $A_{\pm}$ $B_{\pm}$ $C_{\pm}$ in Eq. (27) are calculated through Eqs (28), (29) and (30). The known boundary conditions c_{+} b_{+} c_{-} b_{-} in Eqs (29) and Eq. (30) can be calculated through Eqs (45) and Eq. (46). a_{+} a_{-} in Eq. (28) can be obtained though Eqs (14) and Eq. (33). The first item of the Eq. (21) $(h \star p)(i)$ is the filtered projection calculated from projections without extrapolation [19,1]. After getting the results of Eq. (21), the back-projection process can be done according to reference [19] or for cone-beam situation [1] to produce the reconstructed image.

3. Comparison of various algorithm calculation times

If convolution has been implemented through the FFT algorithm, the number of calculations required for filtering the projections without extrapolation is given by:

$$C_{\text{without}} = K\,N\,\log(N) \tag{47}$$

where K is constant, depending on the implementation (the ideal value of K is 1). N is the length of projection data, for example 512. The calculations $g(i)$ in Eq. (27) for each i are about 20 times (addition and multiplication). To make a comparison, the algorithm introduced above is referred as the fast extrapolation and the extrapolation doubling the length is referred as the normal extrapolation. For the fast extrapolation algorithm, the number of the calculations for filtering process is

$$C_{\text{fast}} = K\,N\,\log(N) + 2\,J\,N \tag{48}$$

The first term of the above formula is the calculation of the convolution with FFT, which is the same as Eq. (47). $J \approx 20$ for the mixed extrapolation.

The Implementation of the normal extrapolation is straightforward. In this case, the length of projection data required is doubled, thus, if the convolution is implemented with FFT the calculations are

$$C_{\text{normal}} = K\,2\,N\,\log(2\,N) \tag{49}$$

We have analyzed the speeds using dual Intel (R) Xeon processors. The software used was C++ Builder 6. The length of the projection was $N = 512$. For the above 3 situations, the average calculation time for 20 samples are shown in the Table 1. The Eqs (48) and (49) together with Table 1 tell us, when

Table 1
The calculation time for different extrapolation algorithms

Algorithms:	Normal extrapolation	Without extrapolation	Fast extrapolation
Calculation time (ms)	31.35	15.65	15.85

N is large, the normal extrapolation spends about twice the calculation time as the fast extrapolation algorithm; the fast extrapolation algorithm spends nearly the same calculation time as the case without extrapolation. Hence the fast extrapolation algorithm is about 2 times faster compared to the normal extrapolation algorithm.

The calculation time determined here, only includes the calculations for the filtering process; the calculation time for the back-projection process was not determined. It is the same for all the three situations. Originally back-projection required more calculations compared to the filtering process. Increasing the speed of the filtering process will have no significant contribution to the whole calculations of the reconstruction. Recently, fast back-projection algorithm [18] appears, where the filtering process and back-projection process will have similar calculations. Hence speeding up the filtering process will have important contribution to the whole calculations of the reconstruction.

4. Application of the mixed extrapolation to two examples

4.1. Example 1

In order to compare the distances of the reconstruction using different extrapolations the simulated parallel projections is used instead of cone-beam measured projections. Standard Shepp-Logan head phantom (Fig. 4a) was used to test the reconstruction results. The image size was chosen as 512×512. The width of the image was defined as 1 $length - unit$. The number of projections was 180. Figure 4b shows the crop of the phantom, which is on the ROI. The ROI corresponds to the FOV of the detector. The crop of the phantom was used as a reference to compare with other reconstructed images. The width of the FOV was chosen as 0.5 $length - unit$. The radius of corresponding ROI is equal to the half of the FOV, which is just the quarter of the width of the image. Parallel projections are simulated from Radon transform of the phantom. The space between two elements of projection was chosen as the distance between two pixels of the image. Truncated projections were obtained by reducing the number of elements of the detector (257) and setting zeros to the outside. Truncated projections were utilized as the input of the reconstruction with extrapolation and without extrapolation.

Figure 4c is the reconstruction without extrapolation. This is referred as "zero" extrapolation. From this image, the artifacts of truncation can be seen clearly, which are bright ring close to the boundary of the ROI of the image. Figure 4d is the reconstruction with constant extrapolation. The constant extrapolation is obtained through substituting $a_{\pm} = 0$, $b_{\pm} = 0$, $\alpha L >> 1$. This image is over corrected from Fig. 4c. The dark ring at the boundary of the ROI can be seen clearly. Figure 4e is the reconstruction with quadratic extrapolation through choosing $L\alpha >> 1$ in Eq. (19). Figure 4f is the reconstruction with mixed extrapolation; here $L = 128$, $m = 1$, $\alpha = 0.73$. Figure 4g is the reconstruction with mixed extrapolation; here $L = 128$, $m = 2$, $\alpha = 0.5$.

In order to compare the reconstructed images with original phantom, similar to the reference [9], the distance from the reconstructed image Y_{ij} to original image X_{ij} is defined as following:

$$d = \frac{\sum_{i=1}^{I} \sum_{j=1}^{I} |Y_{ij} - X_{ij}|^2}{\sum_{i=1}^{I} \sum_{j=1}^{I} |X_{ij} - \bar{X}|^2} \tag{50}$$

Table 2
The distances correspond different extrapolations. The truncated projections are produced with Shepp-Logan head phantom

Extrapolation	zero	constant	quadratic	Mix 1	Mix 2	Ideal
α				0.73	0.5	
Distances	7.2290	0.5941	0.1345	0.0194	0.0173	0.0154

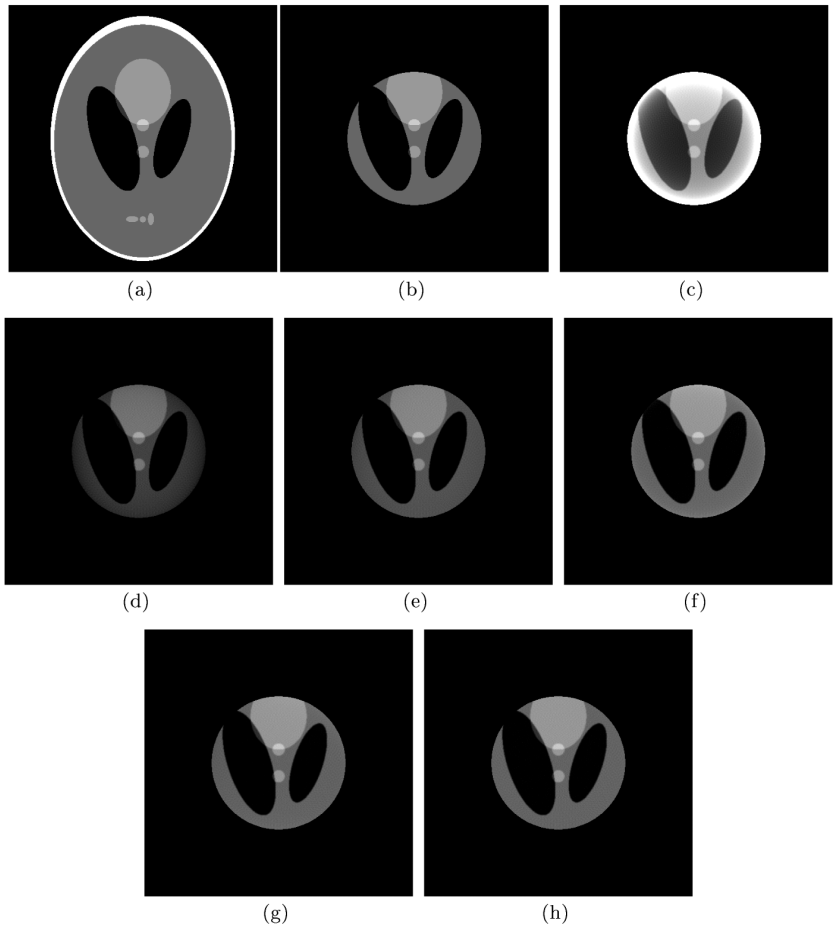

Fig. 4. (a) Shepp-Logan head phantom. (b) The crop of the phantom. (c) The reconstruction without extrapolation. (d) The reconstruction with constant extrapolation. (e) The reconstruction with quadratic extrapolation. (f) the reconstruction with mixed extrapolation; here $L = 256$, $m = 1$, $\alpha = 0.73$. (g) the reconstruction with mixed extrapolation; here $L = 256$, $m = 2$, $\alpha = 0.5$. (h) the crop of the reconstruction with FBP method using non-truncated projections, which was utilized for comparison.

where $\bar{X}$ is average of the image X_{ij}. I is the size of image in one dimension.

Table 2 gives the distances of the reconstruction corresponding different extrapolations. The truncated projections are produced using Shepp-Logan head phantom. In the table "zero" corresponds non-extrapolation; "constant" corresponds constant extrapolation; "quadratic" corresponds quadratic extrapolation; "mix 1" corresponds mixed extrapolation with $m = 1$; "mix 2" corresponds mixed extrapolation with $m = 2$; Ideal corresponds the reconstruction with non-truncated projections. The parameter

Table 3
The distances corresponding to different extrapolations. The truncated projection is produced with modified Shepp-Logan head phantom

Extrapolation	zero	constant	quadratic	Mix 1	Mix 2	Ideal
α				0.73	0.5	
Distances	2.0954	0.2436	0.0492	0.0117	0.139	0.0129

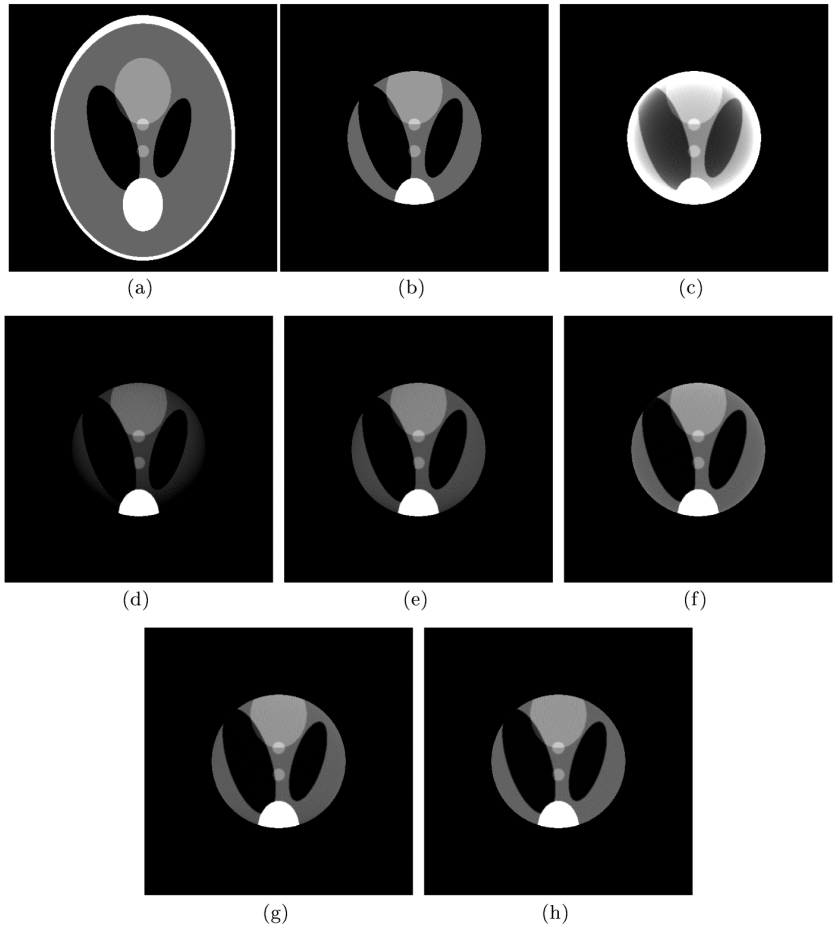

Fig. 5. (a) Modified Shepp-Logan head phantom. (b) The crop of the phantom. (c) The reconstruction without extrapolation. (d) The reconstruction with constant extrapolation. (e) The reconstruction with quadratic extrapolation. (f) The reconstruction with mixed extrapolation; here $L = 256$, $m = 1$, $\alpha = 0.73$. (g) the reconstruction with mixed extrapolation; here $L = 256$, $m = 2$, $\alpha = 0.5$. (h) the crop of the reconstruction with FBP method, which was utilized for comparison.

α in Table 2 is chosen to minimize the distance d in Eq. (50).

4.2. Example 2

In order to study effect of the extrapolations in case that there is a massive object on the border of the ROI, modification is made for the standard phantom through adding up an arm structure of human to the standard phantom. Figure 5a is modified Shepp-Logan head phantom. Other figures from Fig. 5b

to Fig. 5g are similar to Fig. 4 except they are with modified Shepp-Logan head phantom5a instead of standard Shepp-Logan head phantom.

Table 3 is similar to Table 2 except the truncated projections are produced using modified Shepp-Logan head phantom. The distances of mixed extrapolation are 0.0117 and 0.0139, which are very close to ideal distance 0.0129. This means that even for the modified Shepp-Logan head phantom, the reconstructions with mixed extrapolations are almost perfect.

5. Conclusions and future work

For the examples of truncated projections the improved reconstruction results can be obtained with constant and linear extrapolations [14], however, further improved results can be achieved through the mixed extrapolations introduced in this paper.

For implementation of mixed extrapolations, doubling the length of the projections has been avoided. Almost the same calculation time with the extrapolation is achieved comparing the algorithm without extrapolation.

It is remarkable that the extrapolation algorithms for the LFOV problem is not solved thoroughly. If a massive object is added to Shepp-Logan head phantom and it is completely outside the FOV of the detector, the truncation artifacts cannot be eliminated by any extrapolation algorithms, including the mixed extrapolation introduced in this paper. Further study on this is required [14,15].

Acknowledgment

The outhor would like to thank Prof. David A. Jaffray, Prof. Jeffrey H. Siewerdsen for their valuable discussion and feedback.

Appendix

Appendix 1. the details about a_+

$$[a_+(i-(j-1))^2 + b_+(i-(j-1)) + c_+]|_{i=j+L} = 0$$

or

$$a_+(L+1)^2 + b_+(L+1) + c_+ = 0$$

or

$$a_+ = -\frac{b_+(L+1) + c_+}{(L+1)^2}$$

Appendix 2. the details about $g_\pm(i)$

Substitute Eqs (11) to (22), keep in mind that L should be replace as L_+ later. We take $m = 1$ as example.

$$g_+(i) = \sum_{l=j}^{l=j+L_+} h(i-l)\Pi_{L_+}(l-j)[a_+(l-(j-1))^2 + b_+(l-(j-1)) + c_+]$$
$$\cdot \exp(-\frac{l-j}{\alpha L})$$

Let $n = l - j$ or $l = j + n$, we get

$$g_+(i) = \sum_{n=0}^{L_+} h((i-j)-n)\Pi_{L_+}(n)[a_+(n+1)^2 + b_+(n+1) + c_+]$$
$$\cdot \exp\left(-\frac{n}{\alpha L}\right)$$

or

$$g_+(i) = \sum_{n=0}^{L_+} h((i-j)-n)[a_+(n+1)^2 + b_+(n+1) + c_+]$$
$$\cdot \exp\left(-\frac{n}{\alpha L}\right)$$

Consider the function $h(n)$ is symmetric [19], i.e.:

$$h(n) = h(-n)$$

$$g_+(i) = \sum_{n=0}^{L_+} h(n+t)[a_+(n+1)^2 + b_+(n+1) + c_+]$$
$$\cdot \exp\left(-\frac{n}{\alpha L}\right)$$

where we have take $t = j - i$. Considering

$$\begin{aligned} & a_+(n+1)^2 + b_+(n+1) + c_+ \\ &= a_+[(n+t) + (1-t)]^2 + b_+[(n+t) + (1-t)] + c_+ \\ &= a_+[(n+t)^2 + 2(n+t)(1-t) + (1-t)^2] + b_+[(n+t) + (1-t)] + c_+ \\ &= a_+(n+t)^2 + [2a_+(1-t) + b_+](n+t) + [a_+(1-t)^2 + b_+(1-t) + c_+] \end{aligned}$$

and

$$\begin{aligned} & \exp\left(-\tfrac{n}{\alpha L}\right) \\ = \ & \exp\left(-\tfrac{(n+t)+(-t)}{\alpha L}\right) \\ = & \exp\left(-\tfrac{n+t}{\alpha L}\exp(-\tfrac{-t}{\alpha L}\right) \end{aligned}$$

We have

$$g_+(i) = \sum_{n=0}^{L_+} h(n+t)\{a_+(n+t)^2 + [2a_+(1-t) + b_+](n+t)$$

$$+[a_+(1-t)^2+b_+(1-t)+c_+]\}\cdot\exp\left(-\frac{n+t}{\alpha L}\right)\exp\left(-\frac{-t}{\alpha L}\right)$$

or

$$g_+(i)=\sum_{n=t}^{L_++t}h(n)\{a_+n^2+[2a_+(1-t)+b_+]n$$
$$+[a_+(1-t)^2+b_+(1-t)+c_+]\}\cdot\exp\left(-\frac{n}{\alpha L}\right)\exp\left(-\frac{-t}{\alpha L}\right)$$

Define

$$G^{(k)}_{L_+}(t)=\sum_{n=t}^{L_++t}h(n)n^k\exp\left(-\frac{n}{\alpha L}\right)$$

$$g_+(i)=\{a_+G^{(2)}_{L_+}(n)+[2a_+(1-t)+b_+]G^{(1)}_{L_+}(n)$$
$$+[a_+(1-t)^2+b_+(1-t)+c_+]G^{(0)}_{L_+}(n)\}\cdot\exp\left(-\frac{-t}{\alpha L}\right)$$

Define

$$A_+=a_+$$
$$B_+=2a_+(1-t)+b_+$$
$$C_+=a_+(1-t)^2+b_+(1-t)+c_+$$

We have

$$g_+(i)=\{A_+G^{(2)}_{L_+}(t)+B_+G^{(1)}_{L_+}(t)+C_+G^{(0)}_{L_+}(t)\}$$
$$\cdot\exp\left(-\frac{-t}{\alpha L}\right)$$

Appendix 3. the details about $R_\pm$, $S_\pm$

Points line fit method is used. The Fig. 3 Shows the right side. We assumes the direction of i is in the negative direction of the j.

The first five points is used to fit the line:

$$R+Si=f(i)\ \ i=0,1,2,3,4$$

$$R+S\cdot 0=f(0)$$
$$R+S\cdot 1=f(1)$$
$$R+S\cdot 2=f(2)$$
$$R+S\cdot 3=f(3)$$
$$R+S\cdot 4=f(4)$$

Or

$$VB = F$$

Where

$$V = \begin{bmatrix} 1\,0 \\ 1\,1 \\ 1\,2 \\ 1\,3 \\ 1\,4 \end{bmatrix} \qquad B = \begin{bmatrix} R \\ S \end{bmatrix} \qquad F = \begin{bmatrix} f(0) \\ f(1) \\ f(2) \\ f(3) \\ f(4) \end{bmatrix}$$

$VB = F$ can be rewritten as

$$V^T VB = V^T F$$

$$V^T V = \begin{bmatrix} 1\,1\,1\,1\,1 \\ 0\,1\,2\,3\,4 \end{bmatrix} \begin{bmatrix} 1\,0 \\ 1\,1 \\ 1\,2 \\ 1\,3 \\ 1\,4 \end{bmatrix}$$

$$= \begin{bmatrix} 1+1+1+1+1 & 1+2+3+4 \\ 1+2+3+4 & 1+2^2+3^2+4^2 \end{bmatrix}$$

$$= \begin{bmatrix} 5 & 10 \\ 10 & 30 \end{bmatrix}$$

So that we have

$$[V^T V]^{-1} = \begin{bmatrix} 0.6 & -0.2 \\ -0.2 & 0.1 \end{bmatrix}$$

$$V^T F = \begin{bmatrix} 1\,1\,1\,1\,1 \\ 0\,1\,2\,3\,4 \end{bmatrix} \begin{bmatrix} f(0) \\ f(1) \\ f(2) \\ f(3) \\ f(4) \end{bmatrix}$$

$$= \begin{bmatrix} f(0)+f(1)+f(2)+f(3)+f(4) \\ 1f(1)+2f(2)+3f(3)+4f(4) \end{bmatrix}$$

$$= \begin{bmatrix} \sum_{i=0}^{4} f(i) \\ \sum_{i=1}^{4} if(i) \end{bmatrix}$$

So that

$$B = [V^T V]^{-1} V^T F = \begin{bmatrix} 0.6 & -0.2 \\ -0.2 & 0.1 \end{bmatrix} \begin{bmatrix} F_1 \\ F_2 \end{bmatrix}$$

Where

$$F_1 = \sum_{i=0}^{4} f(i)$$

$$F_2 = \sum_{i=1}^{4} if(i)$$

Hence we have

$$R = 0.6F_1 - 0.2F_2$$

$$S = -0.2F_1 + 0.1F_2$$

For the right side extrapolation we consider

$$f(i) = p(-(i - (j - 1)))$$

For the left side extrapolation we consider

$$f(i) = p(i - (k + 1))$$

Considering the direction of the above formula; see Fig. 3, we have

$$R_{\pm} = R$$

$$S_{\pm} = -S$$

or

$$R_{\pm} = 0.6F_1 - 0.2F_2$$

$$S_{\pm} = 0.2F_1 - 0.1F_2$$

References

[1] L.A. Feldkamp, L.C. Davis and J.W. kress, Practical cone-beam algorithm, *J Opt Soc Am A* **1**(6) (June 1984), 612–619.

[2] B.D. Smith, Image reconstruction from cone-beam projections: 'Necessary and sufficient conditions and reconstruction methods, *IEEE trans Med Imaging* **MI-4**(1) (14–25 March 1985).

[3] P. Grangeat, Mathematical framawork of cone beam 3d reconstruction via the first derivative of the Radon transform, in: *Mathematical Methods in Tomography*, G.T. Herman, A.K Louis and F. Natterer, eds, Springer Kerlag, 1990.

[4] K.T. Smith, Reconstruction formulas in computed tomography, in *Proc Symp Appl Math* **27** (1982), 7–23.

[5] D.A. Jaffray, J.H. S.J.W. Wong and A.A. Martinez, Flat-Panel Cone-beam Computed Tomography for image guided radiation Therapy, *Int J Radiation Oncology Biol Phys* **53**(5) (2002), 1337–1349.

[6] A. Faridani, erk L. Ritman and k.T. Smith, Local Tomography SIAM, *J Appl Math* **52**(2) (April 1992), 459–484.

[7] Ref. 7 F .Rashid-Farrokhi, K.J.R. Liu, C.A. Berenstein and D. Walnut, Wavelet-based Multiresolution Local Tomography, *IEEE Transactions on Image Processing* **6** (1997), 1412–1430.

[8] M. Nilsson, Local Tomography at a Glance, Licentiate Theses in Mathematical Sciences 2003:3 ISSN 1404-028X, ISBN91-628-5741-X, LUTFMA-2007-2003. Printed in Sweden by KFS AB Lund, 2003.

[9] P.S. Cho, A.D. Rudd and R.H. Johnson, Cone-beam CT from width truncated projections, *Computerized Medical Imaging and Graphics* **20**(1) (1996), 49–57, 49–57.

[10] F. Noo, R. Clackdoyle and J.D. Pack, A two-step Heilbert transform method for 2D image reconstruction, *Phys Med Biol* **49** (2004), 3903–3923.

[11] K.J. Ruchala, G.H. Olivera, J.M. Kapatoes, P.J. Reckwerdt and T.R. Mack TR, methods for improving limited field-of-view radiotherapy reconstructions using imperfect a priori images, *Med Phys* **29**(11) (Nov 2002), 2590–605.
[12] M.M. Seger, Rampfilter implementation on truncated projection data. Application to 3D linear tomography for logs, *Proceedings SSAB02, Symposium on Image Analysis*, Lund, Sweden, 7-8 March 2002. Editor Astrom.
[13] B. Ohnesorge, T. Flohr, K. Schwartz, J. Heiken and K. Bae, Efficient correction for CT image artifacts caused by objects extending outside the scan field of view, *Med Phys* **27** (2000), 39–46.
[14] S. Zhao and D. Jaffray, Iterative reconstruction-reprojection for truncated projections, AAPM:SU-DD-PDS-19, *Med Phys* **31** (2004), 1719.
[15] S. Zhao, K. Yang, D. Jiang and X. Yang, Interior Reconstruction Using Local Inverse, *Journal of X-Ray Science and Technology* **18** (2010) 1–22.
[16] S. Zhao and H. Halling, Reconstruction of Cone Beam Projections with Free Source Path by a Generalized Fourier Method, published in Proceedings of the International Meeting on Fully, *Three-Dimensional Image Reconstruction in radiology and Nuclear medicine* **2** (1995), P323.
[17] S. Zhao and A. Horst Halling, New fourier transform method for fan beam tomography, published in Nuclear Science Symposium and Medical imaging Conference, *IEEE* **2** (1995), 1287–1291.
[18] A. Brandt, J. Mann, M. Brodski and M. Calun, A fast and accurate multilevel inversion of the radon transform, *Siam J Appl Math* **60**(2), 437–462.
[19] A.C. Kak and M. Slaney, Algorithms for Reconstruction with Nondiffracting Sources, *Section 3 of Principles of Computerized Tomographic Imaging*, IEEE Press, 1988.
[20] Y. Zou and X. Pan, Exact image reconstruction on PI-lines from minimum data in helical cone-beam CT, *Physics in Medicine and Biology* **49**(6) (2004), 941–959.
[21] S. Basu and Y. Bresler, O(n log n) filtered backprojection reconstruction algorithm for tomography, *IEEE Trans Image Processing* **9** (Oct 2000), 1760–1773.
[22] L. Zeng and X. Zou, Katsevich-type reconstruction for dual helical cone-beam CT, *Journal of X-Ray Science and Technology* **18** (2010), 353–367.
[23] J. Wang and L. Xing, A binary image reconstruction technique for accurate determination of the shape and location of metal objects in x-ray computed tomography, *Journal of X-Ray Science and Technology* **18** (2010), 403–414.
[24] B. Lee, H. Lee and Y.G. Shin, Fast hybrid CPU- and GPU-based CT reconstruction algorithm using air skipping technique, *Journal of X-Ray Science and Technology* **18** (2010), 221–234.
[25] L. Zeng, B. Liu, L. Liu and C. Xiang, A new iterative reconstruction algorithm for 2D exterior fan-beam CT, *Journal of X-Ray Science and Technology* **18** (2010), 267–277.
[26] 5.Dan Xia, S. Cho and X. Pan, Image reconstruction in reduced circular sinusoidal cone-beam CT, *Journal of X-Ray Science and Technology* **17** (2009), 189–205.
[27] T. Liu and J. Xu, Differential reconstruction for planar object in computed tomography, *Journal of X-Ray Science and Technology* **17** (2009), 101–114.
[28] L. Li, K. Kang, Z. Chen, L. Zhang and Y. Xing, A general region-of-interest image reconstruction approach with truncated Hilbert transform, *Journal of X-Ray Science and Technology* **17** (2009), 135–152.